
PLASMA OSCILLATIONS AND WAVES

Fine Structure of the Emission Spectra of a Relativistic Cherenkov Plasma Maser

I. L. Bogdankevich, I. E. Ivanov, O. T. Loza, A. A. Rukhadze, P. S. Strelkov,
V. P. Tarakanov, and D. K. Ul'yanov

Institute of General Physics, Russian Academy of Sciences, ul. Vavilova 38, Moscow, 119991 Russia

Received March 21, 2002

Abstract—The evolution of the emission spectrum of a relativistic Cherenkov plasma maser is studied both experimentally and numerically. The frequency range of emission is 1.5–6 GHz at a power level of 50 MW and pulse duration of up to 500 ns. It is shown that the relativistic Cherenkov plasma maser is capable of producing both broadband (with a spectrum width of ~ 1 GHz) and narrowband (≈ 40 MHz) microwave pulses with a tunable mean frequency. Calculations by linear theory and numerical simulations provide a satisfactory explanation of the specific features and the time evolution of the spectra observed. It is suggested that the plasma non-linearity is responsible for the experimentally observed shortening of the microwave pulses and the broadening of the emission spectrum. © 2002 MAIK “Nauka/Interperiodica”.

1. INTRODUCTION

In microwave electronics, a wavelength range of ~ 3 cm is traditionally used to study new principles of the microwave generation. This is explained by the fact that the problem of microwave generation is easier to solve in systems with transverse dimensions on the order of the radiation wavelength. For this reason, engineering problems arise in designing compact electrodynamic structures operating in the millimeter wavelength range, whereas devices operating in the 10-cm wavelength range are too cumbersome.

Relativistic Cherenkov plasma masers (RCPMs) were also studied experimentally in a wavelength range of several centimeters. In [1], a plasma microwave amplifier operating at frequencies of 9 and 13 GHz, and, in [2], a tunable RCPM with a radiation frequency from 4 to 28 GHz (i.e., with a wavelength of $\lambda = 7.5$ – 1.1 cm) are described. A review of theoretical and experimental research on plasma relativistic microwave electronics is given in [3]. These studies clarified the physical mechanism for microwave generation—the stimulated Cherenkov emission from a high-current relativistic electron beam (REB) in a plasma waveguide. In this case, an azimuthally symmetric slow plasma wave with the lowest radial index is excited.

The above result was obtained by measuring the microwave frequency at different plasma densities. Recall that, in plasma relativistic microwave devices, a pulsed high-current REB with a pulse duration of 30–1000 ns is injected into a preformed annular plasma. Modern diagnostic techniques allow fairly exact measurements of the REB parameters in the absence of a plasma, as well as the plasma parameters in the absence of an REB. However, it is still impossible to measure the parameters of the electron beam and plasma in the

course of their interaction and the characteristics of the electromagnetic field inside the waveguide. Therefore, the only way to study the characteristics of the beam–plasma interaction is to measure the parameters of the output electromagnetic radiation and the parameters of the REB passed through the plasma waveguide. That is why the measurements of the power and spectrum of the microwave radiation are of great importance.

Relativistic plasma masers differ from their vacuum analogs, first of all, by the possibility of tuning the frequency over a wide range (e.g., from 4 to 28 GHz [2]). The frequency can be tuned by varying the plasma density between the REB pulses.

In order to roughly estimate the emission frequency during one REB pulse, it was proposed to use a calorimetric spectrometer [4]. An important advantage of this device is that the calorimeter measures the microwave spectrum integrated over the pulse duration and over the transverse cross section of the generated microwave beam, i.e., the total energy spectrum of the microwave pulse. Note that spectrometers usually pick up only a small fraction of the total microwave energy. If the radiation spectrum is broad, the spectrum of the total microwave beam can differ from the spectrum of its small fraction. Clearly, of prime interest is to measure the total radiation spectrum and to compare it with numerical calculations. Only after that, one can consider a more complicated problem of studying the radiation spectrum in different points of the microwave beam. Hence, the microwave calorimetric spectrometer provides basic information about the physical mechanism for the interaction of an electron beam with a plasma under given experimental conditions. By using such a spectrometer, it was established, in particular,

that the total energy of the microwave pulse varies only slightly over the entire frequency range [2].

However, along with advantages, such as the broad frequency range (2–40 GHz) and the absolute measurements of the total spectrum, the microwave spectrometer [4] possesses a number of drawbacks. First, the frequency resolution of the device is rather low ($\sim 20\%$), and, second, the spectrometer has no time resolution and measures the spectrum integrated over the entire microwave pulse. This means, e.g., that we do not know what factors are responsible for the measured spectral width. For example, the emission may be broadband during the entire microwave pulse. However, the broad total spectrum may also form due to variations in the mean frequency of a relatively narrow spectrum during the microwave pulse.

Full information about the microwave spectrum can be obtained experimentally as follows. An antenna is placed into the output microwave beam, and the electric signal is fed through a coaxial cable to a fast oscilloscope. At present, fast digital oscilloscopes with frequency bands of up to 6 GHz (e.g., a Tektronix TDS 6604 digital storage oscilloscope) are available. The Fourier analysis of the time evolution of the electric field at some point of the microwave beam gives complete information about its spectrum. In this case, of course, the advantages of the calorimetric spectrometer are lost, because, with this antenna, we measure the spectrum of a small, unknown fraction of the total microwave beam.

To study the radiation spectrum by this technique, we created a new Cherenkov plasma maser operating at relatively low frequencies. We note that the new device is based on the concept of a plasma maser presented in [3]; our purpose was to retain the physical principles of microwave generation that we previously studied in the frequency range 4–28 GHz.

2. EXPERIMENTAL DEVICE

Figure 1 shows the experimental layout, which is the same as in [3]. A high-voltage pulse is applied to the explosive-emission cathode (1) of the accelerator. An REB (2) is injected along the axis of a circular metal waveguide (3) with preformed annular plasma (4). The electron beam and the plasma are in a strong magnetic field with an induction of $B = 0.8$ T; the beam electrons have the longitudinal velocity component only. On the right side of the metal waveguide (3), the electron beam and the plasma are limited by the end of the central conductor (5) of the output coaxial emitter (6). Microwaves are generated in the plasma waveguide, propagate through a vacuum coaxial waveguide (6), and are emitted by a horn (7) into the atmosphere through a dielectric window (8).

In accordance with the results of our previous studies [3], we enlarged the length and diameter of the metal waveguide, as well as the diameters of the annu-

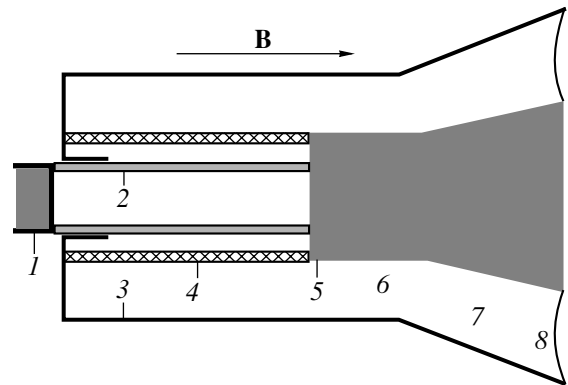


Fig. 1. Schematic of the RCPM: (1) accelerator cathode, (2) REB, (3) metal waveguide, (4) plasma, (5) collector, (6) metal coaxial waveguide, (7) conical coaxial emitting horn, and (8) window.

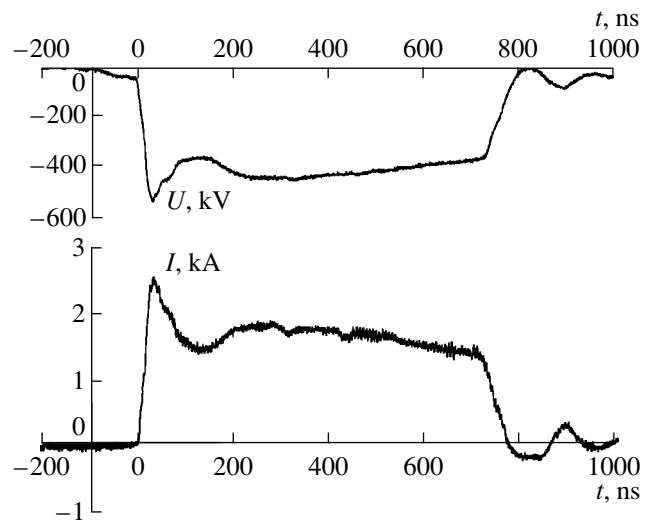


Fig. 2. Waveforms of the voltage pulse at the accelerator cathode U and the REB current I .

lar plasma and the REB. According to calculations, as the plasma density increases from 5×10^{11} to $2.6 \times 10^{12} \text{ cm}^{-3}$, the frequency should increase from 1.5 to 6 GHz.

Figure 2 shows the waveforms of the REB current and the voltage pulse at the accelerator cathode. The pulse duration is 700 ns, the amplitude of the voltage pulse at time $t = 250$ ns is equal to 450 kV, and the current amplitude is 1.8 kA.

The absolute value of the plasma density was not measured. We relied on the results of our previous study [2], in which it was demonstrated that the dependence of the average frequency of the RCPM on the plasma density coincided with calculations. For this reason, in calculations, the density was chosen such

that the calculated mean radiation frequency coincided with the measured mean frequency.

The total energy of the microwave pulse was measured by a wide-aperture calorimeter [5]. The envelope of the microwave pulse power was recorded with a hot-carrier semiconductor detector [6]. These measurements allowed us to trace the time dependence of microwave radiation during the pulse. The radiation frequency averaged over the pulse duration was measured by a calorimetric spectrometer [4].

The techniques for measuring the parameters of the preformed plasma and the diagnostics listed above were also used in our previous studies [3]. In this study, we obtained new experimental data—the time dependences of the radial component of the electric field of microwave radiation $E_r(t)$ for different values of the plasma density. The electric field of radiation was detected by a rod antenna located at a distance of 1 m from the emitting horn. Then, the electric field pulse was led through a cable and a broadband attenuator to the input of a TDS 694C fast oscilloscope with a frequency band of 3 GHz.

When processing the recorded microwave pulse, we considered four time intervals. From the emission spectra calculated for these intervals, we could determine the evolution of the spectrum during the microwave pulse. As an example, Fig. 3 demonstrates signals from the rod antenna and the corresponding spectra of microwave radiation obtained in one pulse at a plasma density of $8 \times 10^{11} \text{ cm}^{-3}$.

3. NUMERICAL SIMULATIONS

The experiment was simulated numerically with the code KARAT [7] by solving Maxwell's equations and the relativistic equation of particle motion. An axisymmetric geometry was used. The electron beam was simulated by the particle-in-cell method. The particles were injected from the left boundary. The time dependences of the electron energy and the electron beam current coincided with experimental dependences shown in Fig. 2. In this numerical model, the diode unit of the device was not considered. The plasma was regarded as a linear medium with time-independent properties. The condition at the right boundary of the metal coaxial waveguide implied that electromagnetic waves were not reflected from it.

The magnetic field induction was $B = 0.8 \text{ T}$, which corresponded to the electron cyclotron frequency $\omega_H = 1.4 \times 10^{11} \text{ s}^{-1}$. The maximum plasma density was $n_p = 1.25 \times 10^{12} \text{ cm}^{-3}$, and the corresponding plasma frequency was $\omega_p = 6.1 \times 10^{10} \text{ s}^{-1}$. Therefore, the condition $\omega_H > \omega_p$ was always satisfied.

In the real experiment, microwave radiation was output through the dielectric window into the atmosphere and the electric field was measured in free space at a distance of $\approx 1 \text{ m}$ from the emitting horn. In numer-

ical simulations, the horn was absent. It was assumed that all the radiation entering the metal coaxial waveguide was completely absorbed at a certain coordinate. Thus, we ignored the reflection from the horn, which took place in the real experiment.

In numerical simulations, we calculated the time dependence of the radial component of the electric field $E_r(t)$ of microwave radiation in the metal coaxial waveguide. Using the calculated dependences $E_r(t)$, we constructed the spectra for the same time intervals as were studied in the experiment.

4. COMPARISON OF THE MEASURED AND CALCULATED EMISSION SPECTRA

Before studying the fine structure of the spectra, we measured the averaged (over the pulse) microwave frequency with the help of the calorimetric spectrometer. It was shown that this frequency can be varied from 2 to 6 GHz at a fixed power of 50 MW by varying the plasma density.

Figure 4 presents the experimental (on the left) and calculated (on the right) spectra of the radial component of the microwave electric field for $n_p = 5.25 \times 10^{11} \text{ cm}^{-3}$. Three phases can be distinguished in the evolution of the measured spectra. During the first 40 ns, broadband radiation with a spectral width of 0.6 GHz is generated. The spectrum consists of individual lines shifted by $\sim 0.1 \text{ GHz}$ from each other. Then, in the time interval 40–80 ns, the spectrum becomes a narrow line with a frequency of 1.5 GHz and width of $\approx 0.04 \text{ GHz}$. Further (in the time interval 80–220 ns), the spectrum broadens again. In the interval 95–180 ns, frequencies from 1.5 to 2.3 GHz are observed and radiation appears at frequencies below 1 GHz. Starting from 180 ns, the spectrum mainly consists of three harmonics with frequencies of 0.9, 1.8, and 2.7 GHz. After 220 ns, the radiation intensity vanishes, although the REB current pulse lasts up to 700 ns.

In simulations, only two phases were observed. In the first phase (up to 80 ns), the spectrum is broad. As in the experiment, the spectrum consists of individual lines shifted by $\sim 0.1 \text{ GHz}$ from each other. Since 100 ns, the spectrum begins to narrow. In the interval 180–220 ns, a relatively narrow line with a frequency of 1.6 GHz and width of 0.06 GHz is observed. Unlike the experiment, in simulations, intense microwave radiation is observed up to the end of the REB current pulse and no spectrum broadening occurs.

Hence, a transition from a broad to a narrow spectrum takes place in both the experiment and simulations. In the experiment, this transition occurs in 40 ns, whereas in simulations, it occurs in 80 ns. Then, in the experiment, we observe the second transition (from a narrow to a broad spectrum) and microwave generation terminates. In simulations, the second transition is absent and the intensity of microwave radiation remains

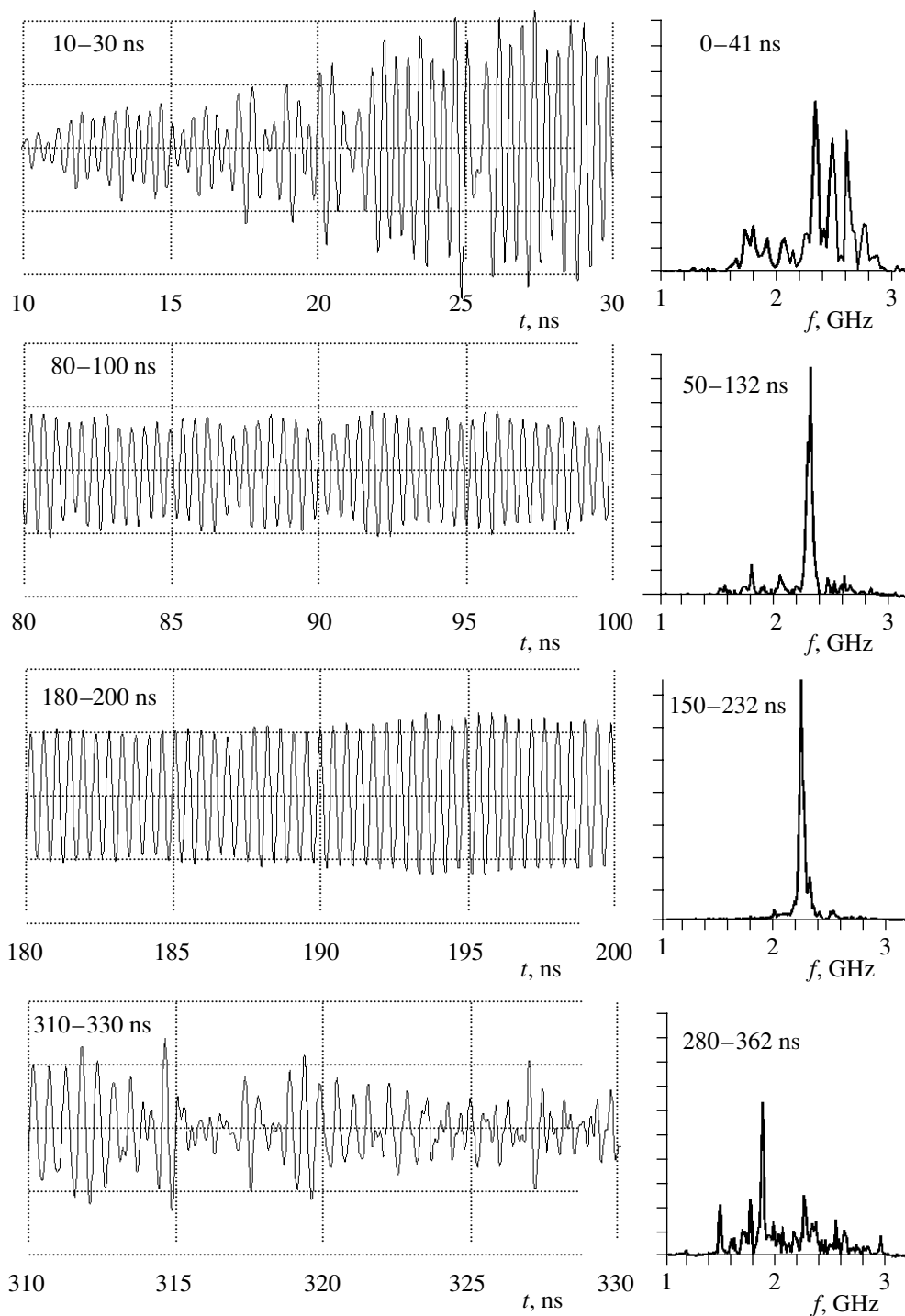


Fig. 3. Fragments of the waveforms of the radial component of the microwave electric field at different delays from the pulse front (on the left) and the spectra calculated from these waveforms (on the right) for $n_p = 8 \times 10^{11} \text{ cm}^{-3}$.

at a constant level up to the end of the REB current pulse.

Figure 5 shows the emission spectra for a plasma density of $n_p = 9 \times 10^{11} \text{ cm}^{-3}$; here, the mean radiation frequency is equal to 2.7 GHz. As in the case of the

lower plasma densities (Figs. 3, 4), two transitions are observed in the experiment: from a broad to a narrow spectrum in the beginning of the pulse (after 40 ns) and back to a broad spectrum after 100 ns. In this case too, only the first transition is present in simulations. The

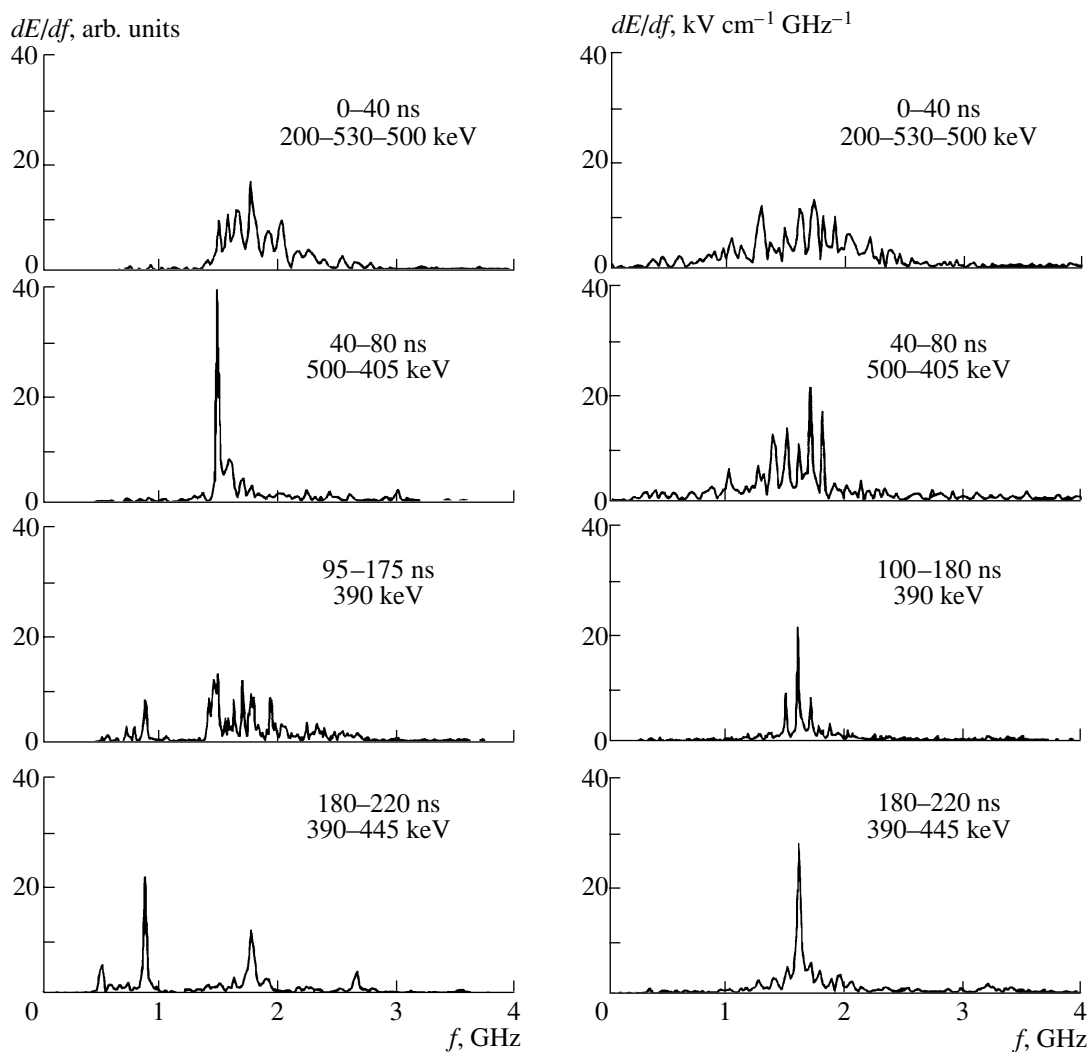


Fig. 4. Microwave spectra for $n_p = 5.25 \times 10^{11} \text{ cm}^{-3}$: experiment (on the left) and simulations (on the right). The time intervals in which each spectrum was calculated and the electron energy ranges within this interval are shown.

calculated spectrum is broad during the first 120 ns; then, it narrows and remains narrow up to the end of the pulse.

Figure 6 demonstrates the spectra for even a higher plasma density: $n_p = 1.25 \times 10^{12} \text{ cm}^{-3}$. In the experiment, we failed to detect a narrowband emission in any time interval under these conditions. In simulations, such narrowband emission appears 240 ns after the beginning of the current pulse, i.e., when the measured radiation intensity already begins to fall.

5. DISCUSSION OF RESULTS

The experimental and simulation results presented above demonstrate the typical features of the RCPM operation. First, the frequency and spectral width of microwave radiation vary with time during the pulse. Second, the wide frequency spectrum generated under

certain conditions consists of individual, relatively narrow lines. Third, the frequency of microwave radiation depends on the plasma density.

The time behavior of radiation during the microwave pulse is illustrated by the waveforms of the microwave electric field (Fig. 3). During the first 40 ns, the radiation frequency decreases from 2.6 GHz to 2.4 GHz, whereas the beam electron energy varies from nearly 200 to 530 keV, which is accompanied by the corresponding increase in the current. Such a dependence of the microwave frequency on the electron energy is explained by Fig. 7, which shows the dispersion curves for the plasma waveguide in the presence of an electron beam with an energy of 530 keV and a current of 2.4 kA (curves 1, 2, 3) and with an energy of 200 keV and a current of 0.6 kA (curves 4, 5, 6). The plasma

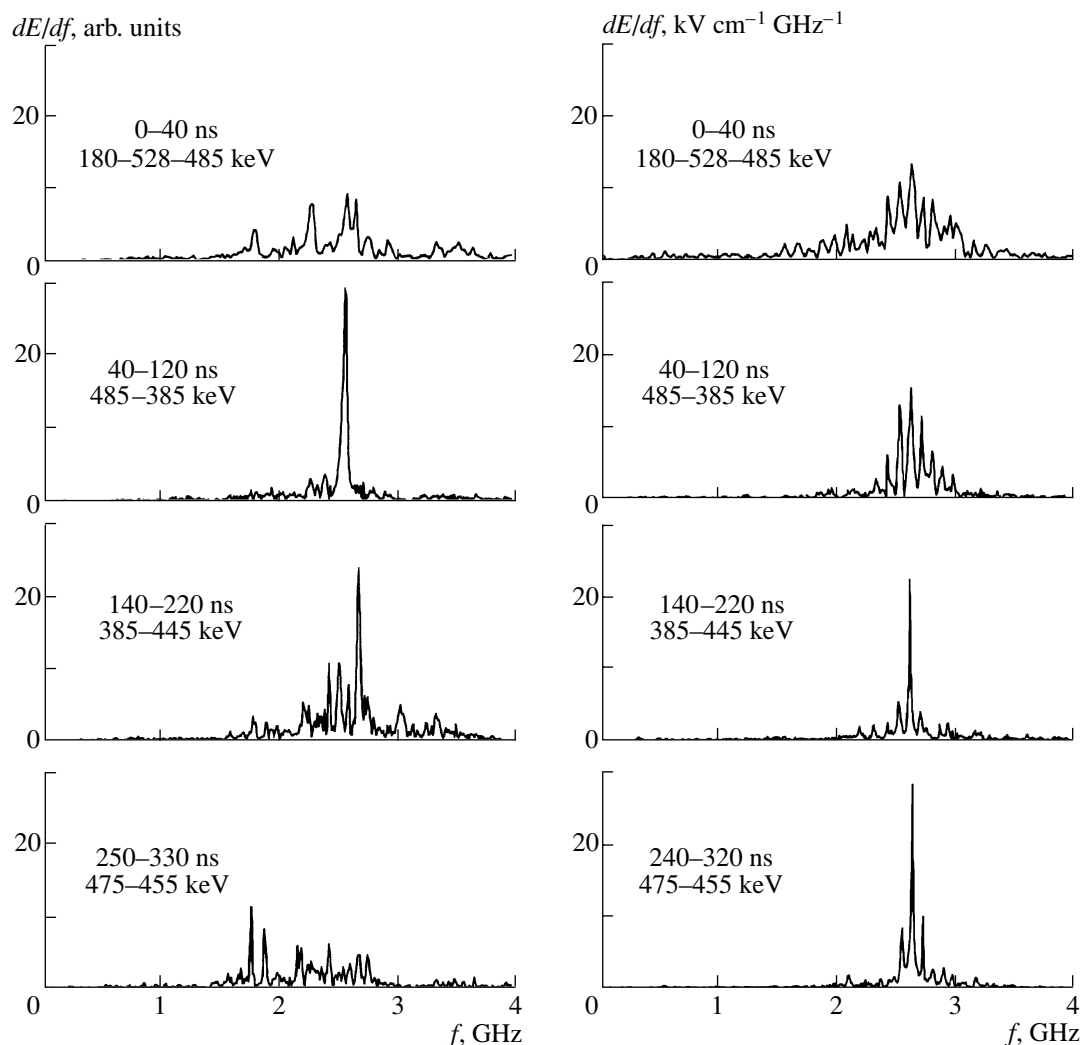


Fig. 5. Microwave spectra for $n_p = 9 \times 10^{11} \text{ cm}^{-3}$: experiment (on the left) and simulations (on the right).

density is $n_p = 8 \times 10^{11} \text{ cm}^{-3}$, which corresponds to the conditions of Fig. 3.

At an electron energy of 530 eV, the system is unstable at all frequencies below ω_1 ; at 200 keV, it is unstable at frequencies below ω_2 . As the electron energy increases, the maximum frequency of the excited oscillations decreases: $\omega_1 < \omega_2$. At the given parameters of the plasma and the electron beam, the frequency decreases by $\omega_2 - \omega_1 \approx 1.8 \times 10^9 \text{ rad/s}$, i.e., by $\approx 0.3 \text{ GHz}$. Microwave generation occurs at a frequency corresponding the maximum value of the linear amplification factor δK . The frequency dependences of δK are shown in Fig. 8 (curves *I*); the maximums of the curves lie near the maximum cutoff frequencies. The change of the maximum frequency by $\approx 0.3 \text{ GHz}$ agree with the change by $\approx 0.2 \text{ GHz}$ of the frequency observed in the experiment.

After 80 ns, the electron energy varies from 400 to 450 keV; correspondingly, the electron beam current

varies as shown in Fig. 2. However, as is easily seen from the above estimates, this cannot lead to a substantial change in the microwave frequency.

At all of the plasma densities (Figs. 3–6), broadband microwave emission is observed during the first 40 ns in both the experiment and simulations. The emission spectrum consists of individual lines shifted by $\sim 0.1 \text{ GHz}$ from each other. It is well known that the maser emits the longitudinal modes satisfying the condition

$$k_z = \frac{N\pi}{L}; \quad (1)$$

where k_z is the longitudinal wavenumber, N is the number of the longitudinal mode, and L is the plasma waveguide length. Hence, the wavenumbers of neighboring longitudinal modes differ by $\Delta k_z = \pi/L$. In a bounded beam-plasma system, the modes are excited for which the amplification factor is topmost, whose frequencies are close to ω_1 and ω_2 (see Fig. 7), and

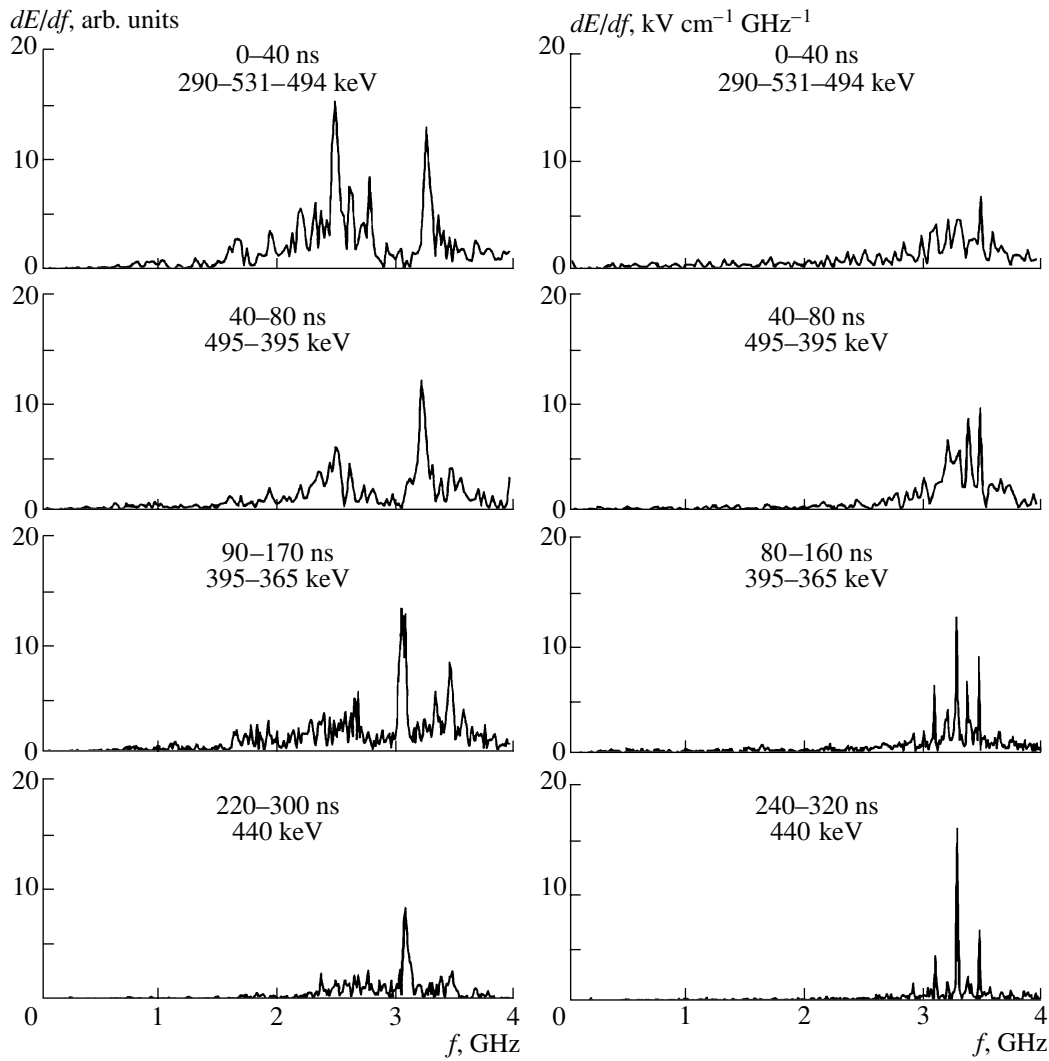


Fig. 6. Microwave spectra for $n_p = 1.25 \times 10^{12} \text{ cm}^{-3}$: experiment (on the left) and simulations (on the right).

whose k_z values satisfy condition (1). It follows from here that the radiation frequency can take discrete values and that the nearest possible frequencies differ by

$$\Delta\omega = \Delta k_z \cdot V_{gr} = \frac{\pi V_{gr}}{L}; \quad (2)$$

where V_{gr} is the group velocity of the plasma wave near the resonant frequency. According to simulations, we have $V_{gr} = 1.8 \times 10^{10} \text{ cm/s}$ and $L = 70 \text{ cm}$. Hence, the difference between the neighboring frequencies is equal to $\delta f = 0.13 \text{ GHz}$. This value nearly coincides with the observed difference between the frequencies of the neighboring spectral lines, $\Delta f \sim 0.1 \text{ GHz}$, in the time interval 0–40 ns in both the experiment and simulations.

Note that the above estimates for δf are rather rough. In particular, no account has been taken of the fact that the wave excited by the beam and the wave reflected

from the collector have different k_z values. Thus, at $n_p = 8 \times 10^{11} \text{ cm}^{-3}$ and the radiation frequency $\omega/2\pi = 2.3 \text{ GHz}$, the k_z value in the direct wave is less than that in the reflected wave by a factor of 1.15 (Fig. 7).

Based on the results of linear theory, we may attempt to explain the radiation spectra observed in the experiment and simulations. To trigger self-oscillations, it is necessary to satisfy the starting conditions for generator excitation:

$$\kappa_l \kappa e^{\delta K \cdot L} > 1; \quad (3)$$

where κ_l and κ are the reflection coefficients from the left and right ends of the plasma waveguide, respectively, and δK is the amplification factor. In simulations, we always assumed $\kappa_l = 1$. Figure 8 shows the δK (curve 1) and κ^2 (curve 2) values calculated in the liner approximation as functions of the radiation frequency f for two values of the plasma density: 5.25×10^{11} and

$1.25 \times 10^{12} \text{ cm}^{-3}$. It should be remembered that, for $n_p = 5.25 \times 10^{11} \text{ cm}^{-3}$ (Fig. 4), the radiation frequency was equal to $\approx 1.6 \text{ GHz}$, whereas for $n_p = 1.25 \times 10^{12} \text{ cm}^{-3}$ (Fig. 6), the frequency was close to 3.3 GHz . The vertical lines in Fig. 8 correspond to the frequencies satisfying conditions (1) and (2); in this case, the longitudinal mode with the number $N = 11$ corresponds to a frequency of 1.6 GHz and $N = 23$ corresponds to a frequency of 3.3 GHz .

In the linear approximation, the frequency range of the beam-plasma instability ($\delta K > 0$) for both plasma densities is sharply bounded at the high-frequency side and extends to zero at the low-frequency side. For $n_p = 5.25 \times 10^{11} \text{ cm}^{-3}$, generation condition (3) is satisfied in the frequency range from 0.4 to 2.5 GHz , and, for $n_p = 1.25 \times 10^{12} \text{ cm}^{-3}$, it is satisfied in the range from 0.8 to 4.5 GHz . Thus, linear theory predicts the excitation of a very broad frequency spectrum.

In contrast, the nonlinear interaction can result in the generation of narrowband emission at $n_p = 5.25 \times 10^{11} \text{ cm}^{-3}$. In this case, microwave generation can be obtained when the amplification factor δK is close to its maximum value and the frequency is close to that corresponding to the maximum δK value. For $n_p = 1.25 \times 10^{12} \text{ cm}^{-3}$, in the frequency range corresponding to generation, the amplification factor δK , as well as the reflection coefficient κ , is substantially higher (Fig. 8). For this reason, the generation of a single longitudinal mode with a narrow frequency spectrum at this plasma density is observed neither in simulations nor in the experiment.

Finally, we discuss the difference between the experimental and simulation results. In the experiment, the so-called “microwave pulse shortening” is observed: microwave generation ceases long before the REB current terminates. This effect is absent in simulations by the code KARAT. In the experiment, we observe the generation of broadband emission just before the end of the microwave pulse. In simulations, this effect is also absent. This difference, in our opinion, may be explained by the fact that the numerical model assumes the plasma response to be linear. The code KARAT enables more adequate simulations in which both the plasma and the electron beam are modeled by the PIC method. We hope that taking into account plasma nonlinearity will allow us to describe both effects—the termination of microwave generation before the end of the current pulse and the broadening of the radiation spectrum immediately before generation terminates.

Effects similar to those mentioned above—the modulation of the amplitude of the microwave pulse and the spectrum broadening—were studied theoretically and experimentally for nonrelativistic electron beams (see review [8] and also [9, 10]). It was shown that, due to plasma nonlinearity, microwave oscillations excite ion oscillations and waves, which causes variations in the

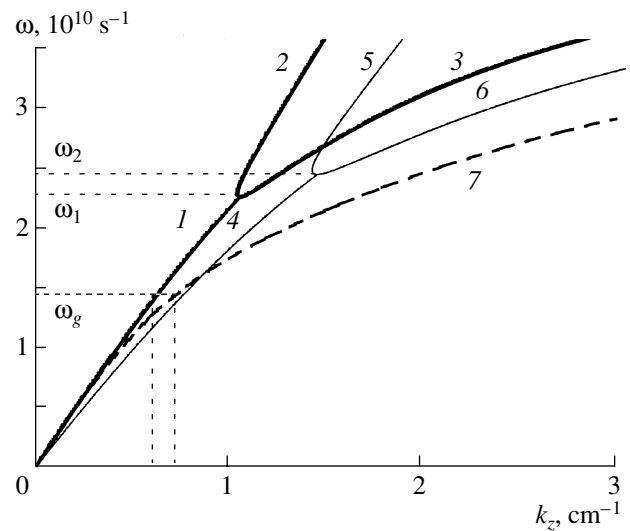


Fig. 7. Dispersion curves for an annular plasma with $n_p = 8 \times 10^{11} \text{ cm}^{-3}$ in a metal waveguide in the presence of an REB with the parameters (1, 2, 3) 530 keV and 2.4 kA and (4, 5, 6) 200 keV and 0.6 kA . Curve 7 is calculated for a plasma without an REB; ω_g is the generated frequency.

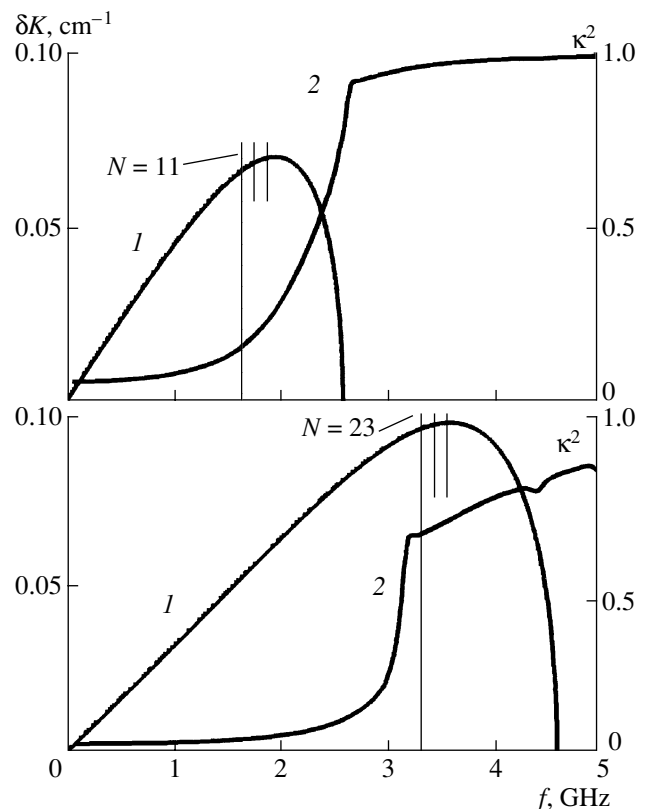


Fig. 8. Frequency dependences of (1) the linear amplification factor δK for an REB with 450 keV and 1.8 kA and (2) the square of the reflection coefficient κ^2 of the plasma wave from the right end of the plasma waveguide for $n_p =$ (a) 5.25×10^{11} and (b) $1.25 \times 10^{12} \text{ cm}^{-3}$.

plasma density; as a result, the plasma becomes non-uniform and unsteady, which can lead to the suppression of microwave oscillations and waves and can significantly change their spectrum. Furthermore, the increase in the thermal velocity of plasma electrons to the wave phase velocity also makes the adopted model inadequate.

We hope to confirm these conclusions and to find ways of reducing the role of nonlinear effects in the RCPM experiments. This is important for applications. Most probably, nonlinear effects will make it hardly possible to create a tunable single-frequency RCPM with a pulse duration much longer than the ion oscillation period (i.e., 100 ns). However, all relativistic microwave sources are pulsed in principle, with a pulse duration of shorter than 1 μ s. The problem of creating a single-frequency RCPM with a pulse duration of up to 1 μ s and tunable over a wide frequency range seems to us quite solvable.

6. CONCLUSIONS

(i) The time evolution of the radiation spectrum during the RCPM pulse has been studied experimentally.

(ii) It is shown that numerical simulations and calculations by linear theory satisfactorily explain the specific features and time evolution of the spectra observed.

(iii) It is shown that the RCPM is capable of producing both broad- and narrowband microwave pulses with a tunable mean frequency.

(iv) It is suggested that the plasma nonlinearity is responsible for the shortening of the microwave pulse and the broadening of the radiation spectrum.

ACKNOWLEDGMENTS

We thank S.D. Korovin for providing us with a TDS-694C fast oscilloscope (without which this study would be impossible). We are also grateful to M.V. Kuzelev and I.N. Kartashov for calculating the curves in Figs. 7 and 8. This work was supported in part

by the Program of the Ministry of Industry, Science, and Technology (MIST) of the Russian Federation under the Program for Supporting Unique Devices (registration no. 01-04); the MIST Scientific Program "Physics of Microwaves" (project no. 1.11); the Complex program of the Presidium of the Russian Academy of Sciences "Generation of High-Power Pulses of Electric Energy, Particles, and Electromagnetic Radiation," project "Broadband RCPM with Microsecond Pulse Duration"; the Russian Foundation for Basic Research (project no. 01-02-17265); and the U.S. Civilian Research and Development Foundation for the Independent States of the Former Soviet Union (CRDF) (grant no. RP1-2269).

REFERENCES

1. A. V. Ponomarev, P. S. Strelkov, and A. G. Shkvarunets, *Fiz. Plazmy* **26**, 633 (2000) [*Plasma Phys. Rep.* **26**, 592 (2000)].
2. P. S. Strelkov and D. K. Ul'yanov, *Fiz. Plazmy* **26**, 329 (2000) [*Plasma Phys. Rep.* **26**, 303 (2000)].
3. M. V. Kuzelev, O. T. Loza, A. A. Rukhadze, *et al.*, *Fiz. Plazmy* **27**, 710 (2001) [*Plasma Phys. Rep.* **27**, 669 (2001)].
4. I. L. Bogdankevich, P. S. Strelkov, V. P. Tarakanov, *et al.*, *Prib. Tekh. Éksp.*, No. 1, 92 (2000).
5. A. G. Shkvarunets, *Prib. Tekh. Éksp.*, No. 4, 72 (1996).
6. M. D. Raizer and L. É. Tsopp, *Radiotekh. Élektron.* (Moscow) **20**, 1691 (1975).
7. V. P. Tarakanov, *User's Manual for Code KARAT* (Springfield, 1992).
8. Ya. B. Faĭnberg, *Fiz. Plazmy* **26**, 362 (2000) [*Plasma Phys. Rep.* **26**, 335 (2000)].
9. Yu. P. Bliokh, M. G. Lyubarskiĭ, and V. O. Podobinskiĭ, *Fiz. Plazmy* **20**, 910 (1994) [*Plasma Phys. Rep.* **20**, 817 (1994)].
10. E. A. Kornilov, O. F. Kovpik, S. M. Krivoruchko, and Ya. B. Faĭnberg, *Fiz. Plazmy* **24**, 1039 (1998) [*Plasma Phys. Rep.* **24**, 971 (1998)].

Translated by N. F. Larionova

SPELL: OK